Measurement and Modeling of Residual Stress-Induced Warping in Direct Metal Deposition Processes

N.W. Klingbeil, J.L. Beuth, R.K. Chin and C.H. Amon
Department of Mechanical Engineering
Carnegie Mellon University
Pittsburgh, PA 15213

Abstract

Tolerance loss due to residual stress-induced warping is a major concern in solid freeform fabrication (SFF) processes. An understanding of how residual stresses develop and how they lead to tolerance loss is a key issue in advancing these processes. In this paper, results are presented from warping experiments on plate-shaped specimens created by microcasting and welding processes used in Shape Deposition Manufacturing (SDM). Results from these experiments give insight into differences between the two processes, the role of preheating and insulating conditions during manufacture and the influence of deposition path on magnitudes and distributions of warping displacements. Results are then compared to predictions from two types of residual stress models. While the models effectively predict warping magnitudes and the effects of various thermal conditions, they are unable to capture some of the more subtle trends in the experiments. Results from the experiments and numerical models suggest that a combination of initial substrate preheating and part insulation can be applied to SDM and similar SFF processes to limit warping deflections, which is substantially simpler than active control of part temperatures during manufacture. Results also suggest that 3-D mechanical constraints are important in achieving precise control of warping behavior in SFF processes.

Introduction

Residual stress-induced warping is a concern in a variety of solid freeform fabrication (SFF) processes, particularly those seeking to build parts directly, without post-processing steps such as sintering or infiltration by a low-melt alloy. One such process is Shape Deposition Manufacturing (SDM), currently under development at Carnegie Mellon University (Merz et al., 1994) and Stanford University (Fessler et al., 1996). Several methods have been investigated for the deposition of fully-dense metals within the SDM process, including microcasting, conventional welding and laser deposition. This paper directly considers the microcasting and welding techniques under development at Carnegie Mellon University. The microcasting deposition process involves the deposition of discrete macroscopic droplets (1/8"-1/4" in diameter) of molten metal, and has been the primary method of material deposition used in SDM. The desire for increased speed and accuracy of material deposition has recently motivated research into welding deposition, where material is deposited in continuous beads using a standard MIG welder. As summarized by Prinz et al. (1997), other SFF techniques under development for direct layered manufacturing of fully-dense metals include Direct Selective Laser Sintering (University of Texas), Laser Engineered Net Shaping (Sandia National Labs) and Directed Light Fabrication (Los Alamos National Labs).

One of the most critical issues in direct deposition of fully-dense metals is residual stress-induced warping, which can lead to unacceptable losses in dimensional tolerance (Prinz et al. (1995), Amon et al. (1998)). Thus, methods are required for measuring and modeling warping, with the goal of understanding the effects on warping of deposition process parameters. Measurement of warping in laser deposition has been considered for beam-shaped deposits by Fessler et al. (1996). The present paper outlines an experimental technique for the systematic measurement of warping in plate-shaped deposits, which allows quantification of warping parallel and transverse to the material deposition direction (Klingbeil et al., 1997 and Klingbeil, 1998). Experimental results are presented for both microcast and welded stainless steel specimens, and the effects on warping of substrate pre-heating and material deposition path are outlined. The experimental results are next compared to numerical model predictions, which are obtained using

the one-dimensional (1-D) axisymmetric and two dimensional (2-D) generalized plane strain (GPS) thermomechanical finite element models of Chin (1998). The thermomechanical models used in this study specifically model the microcasting process and follow those of Chin *et al.* (1995, 1996a, 1996b).

While the experimental and numerical results presented herein relate quantitatively to two metal deposition processes used in SDM, the results offer qualitative insight applicable to other direct layered manufacturing applications. The experimental and numerical results suggest that the effects on warping deformation of substrate pre-heating/insulating conditions and material deposition path can be substantial. Furthermore, results suggest that somewhat subtle differences in mechanical constraints during material deposition can result in significant differences in residual stress generation and subsequent part warping.

Measurement of Warping

The warping measurements discussed herein involve high-precision deflection measurements in conjunction with 2-D polynomial least square fits of the displacement data, which are subsequently used to obtain curvatures. The experimental procedure for obtaining warping deflections follows that of Klingbeil *et al.* (1997), with further details provided in Klingbeil (1998). In brief, molten stainless steel is deposited over a square region onto the surface of a 6" x 6" x 0.47" fully-annealed carbon steel substrate, which is bolted along its edges to prevent warping during manufacture. Following material deposition the specimen is allowed to cool to room temperature, after which the deposit is machined flat to a final thickness of 0.055". The specimen is then unbolted, which results in residual stress-induced warping. The warping deflections are measured using the coordinate measuring capabilities of the CNC milling machine (precise to within ± 0.0001"). Deflection measurements are taken at 81 equally-spaced points forming a 4.0" x 4.0" grid centered on the surface of the deposit. Once the deflections are measured, a 2-D polynomial surface $w(x,y)$ is determined from a 2-D least square curve fit (order n) of the measured deflections, after which the curvatures $w_{,xx}(x,y)$ and $w_{,yy}(x,y)$ in the x and y directions are obtained by analytical differentiation of the function $w(x,y)$. Details of the curve fitting procedures are outlined by Klingbeil (1998). In the upcoming paragraphs, results are presented for both n = 2 and n = 3 least square fits. The n = 2 fits result in uniform curvatures $w_{,xx}$ and $w_{,yy}$, which can be interpreted as average curvatures in the x and y directions. The n = 3 fits allow a bilinear variation in $w_{,xx}$ and $w_{,yy}$, and are highly useful in illustrating deposition path effects. All curvature results are normalized by $\kappa_{max} = 0.00834\,in^{-1}$, the maximum theoretical curvature corresponding to release of a fully-plastic biaxial moment with an assumed room temperature yield stress of 60 ksi (Klingbeil, 1998). Measured deflections are normalized by L = 4.0".

Representative Microcast Specimen Results

Average (n = 2) curvature results are summarized for five microcast specimens in Table 1. Results are presented for three initially room temperature specimens, as well as for two specimens subjected to a uniform 200°C substrate pre-heat prior to material deposition. All microcast specimens are manufactured using a raster deposition path, where material deposition begins in the positive x-y corner and continues back and forth parallel to the x direction. The results of Table 1 indicate that for all specimens, warping is more severe in the x direction (parallel to the deposition direction). On average, uniform substrate pre-heating is seen to decrease warping magnitudes transverse to the deposition direction, however no measurable effect is observed parallel to the deposition direction. The actual measured deflections and corresponding n = 3 least square deflections and curvatures for specimen #1 (no pre-heat) are depicted in Fig. 1. Note that both $w_{,xx}$ and $w_{,yy}$ are greatest at the start of material deposition, and decrease with decreasing values of y (i.e., as the total amount of deposited material increases). This suggests that inherent

substrate pre-heating during material deposition acts to reduce the thermal mismatch, which ultimately results in less warping. Furthermore, n = 3 results for pre-heated specimens (not shown here) indicate that the payoff in decreased values of $w_{,yy}$ is greatest at the start of material deposition, where the substrate would otherwise be comparatively cold. Thus, an initial pre-heat is of greatest advantage for the first few deposited rows, after which the deposition process inherently provides substantial substrate pre-heating.

Table 1. Microcast Specimen Average (n = 2) Curvature Results

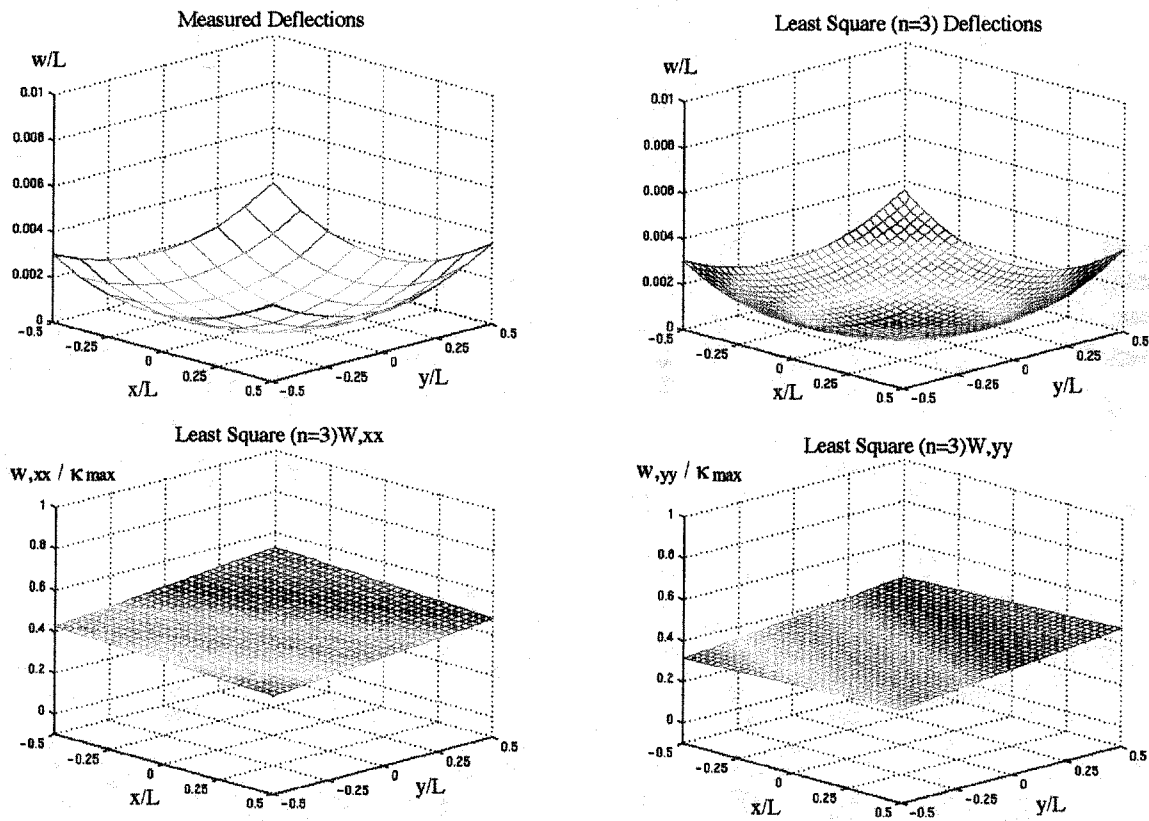| Specimen #	No Pre-Heat			200°C Pre-Heat	
	1	2	3	4	5
$w_{,xx}$ / κ_{max}	0.434	0.478	0.481	0.457	0.483
$w_{,yy}$ / κ_{max}	0.376	0.355	0.397	0.331	0.307

(Note: $\kappa_{max} = 0.00834 \, in^{-1}$)

Figure 1. Representative Measured and Least Square (n = 3) Microcast Results

Representative Welded Specimen Results

Average (n = 2) curvatures are presented for five welded specimens in Table 2. Results are presented for three deposition paths: the raster path used for microcast specimens, an outside-in spiral path and an inside-out spiral path. The outside-in path begins in the positive x-y corner and continues in a spiral fashion until ending in the center, while the inside-out path begins in the center and ends in the positive x-y corner. The measured deflections and n = 3 results are depicted for a raster path specimen (specimen #1) in Fig. 2. Note the strong decrease in $w_{,xx}$ and $w_{,yy}$ during material deposition. While n = 3 results for the spiral deposition paths (not shown here) indicate

much more uniform warping, the resulting average (n = 2) curvatures in Table 2 are substantially larger than those obtained with the raster path. This is because the spiral paths fail to take full advantage of inherent substrate pre-heating, which for the raster path significantly reduces the average warping. A comparison of Figs. 1 and 2 indicates more strongly decreasing curvatures (i.e., more inherent substrate pre-heating) in welding than in microcasting. As a result, the average (n = 2) curvatures for the raster path specimens of Table 2 are much lower than the microcast results of Table 1. It should finally be noted that as observed for microcasting, results for the welded raster path specimens indicate greater warping parallel to the deposition direction.

Table 2. Welded Specimen Average (n = 2) Curvature Results

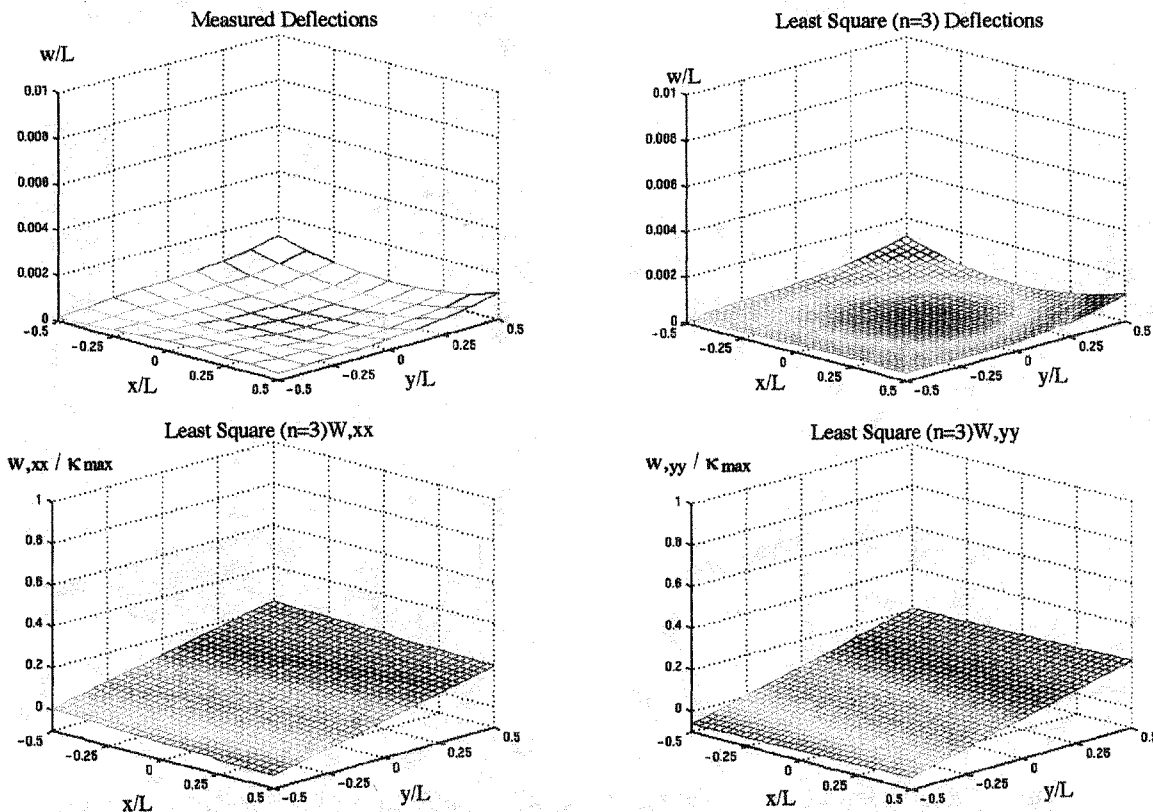| Specimen # (Path)	1 (Raster)	2 (Raster)	3 (Outside-In)	4 (Inside-Out)	5 (Inside-Out)
$w_{,xx}$ / κ_{max}	0.0933	0.0948	0.151	0.302	0.300
$w_{,yy}$ / κ_{max}	0.0784	0.0734	0.197	0.270	0.283

(Note: $\kappa_{max} = 0.00834\ in^{-1}$)

Figure 2. Representative Measured and Least Square (n = 3) Welded Raster Path Results

Implications of the Measured Results

Several practical implications for direct metal deposition processes are evident from the experimental results. First of all, results suggest that when depositing in a raster path, material should not be deposited parallel to the longest part dimension. Because the curvature is greatest parallel to the deposition direction, depositing parallel to the longest part dimension would result in greater warping deflections and loss of tolerance. Secondly, it is advisable to use a deposition path which takes full advantage of inherent substrate preheating. While spiral paths result in more uniform warping, raster paths are more effective for pre-heating the substrate. Finally, the

experimental results suggest that a uniform substrate pre-heating prior to material deposition can be used to gain an initial advantage, after which the process provides substantial substrate heating.

Modeling of Warping

Modeling warping in deposited metals is facilitated by the following key ideas. During material deposition, the deposit and substrate are constrained from warping and the resulting residual stress state is determined by high-temperature nonlinear material response. Following manufacture, the plate is released from its constraints, which results in primarily elastic unloading. Thus, given the constrained residual stress state, subsequent warping can be predicted by an elastic analysis. In this study, the 1-D axisymmetric and 2-D generalized plane strain (GPS) thermomechanical finite element models of Chin (1998) are used to model the constrained residual stress state for a thin layer of stainless steel deposited onto a carbon steel substrate. As previously mentioned, the numerical models are designed to approximate residual stresses in microcasting. The 1-D models effectively represent an entire layer deposited at once (Fig. 3a), and predict upper bounds on warping in microcast deposits (Chin *et al.* 1996a). The GPS models are used in this study to model a single deposited layer composed of five successively deposited rows (Fig. 3b). As opposed to the 1-D models, the GPS models can account for deposited row free-edge effects as well as substrate pre-heating occurring during material deposition. In addition, they enable a comparison of the warping curvatures parallel and transverse to the deposition direction.
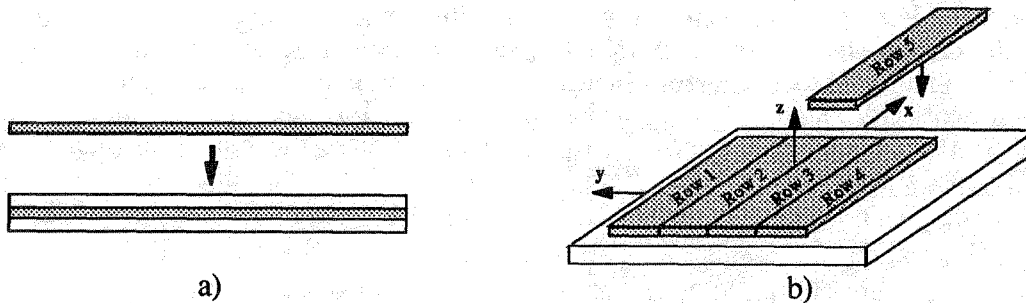

a)   b)

Figure 3. Physical Interpretation of a)1-D Axisymmetric and b) GPS Models

1-D Axisymmetric Models

The 1-D numerical modeling procedures used here follow those described in detail by Chin *et al.* (1996a). A schematic of the 1-D axisymmetric model geometry and boundary conditions is depicted in Fig. 4.
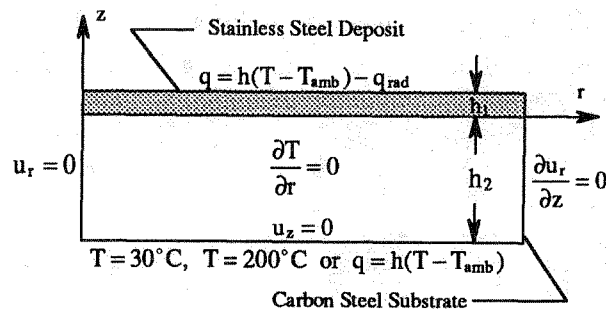

Figure 4. 1-D Axisymmetric Model Geometry and Boundary Conditions

In brief, an initially molten stainless steel deposit is bonded to an initially room temperature carbon steel substrate, after which the deposit and substrate are allowed to cool to room temperature. Both the deposit and substrate are assumed to have elastic-perfectly plastic constitutive behavior, with temperature-dependent elastic properties and yield strengths (Chin *et al.* 1996a). The thicknesses of the stainless steel deposit and carbon steel substrate are $h_1 = 0.055"$ and $h_2 = 0.470"$,

respectively, which are in keeping with the final dimensions of the warping specimens previously discussed. The mechanical constraints are meant to approximate the bolted constraints in the experiments (i.e., no warping). The thermal model used is one-dimensional, with appropriate boundary conditions applied to the top and bottom surfaces. As seen in Fig. 4, three separate thermal boundary conditions on the bottom surface of the substrate are considered: a fixed temperature of $T = 30°C$, a fixed temperature of $T = 200°C$, and a convection condition. Compared to the fixed temperature conditions, the convection condition is nearly equivalent to thermal insulation. The 1-D axisymmetric models predict an equal biaxial constrained residual stress distribution $\sigma_r(z)$, which can be readily used in obtaining curvatures. As outlined in Klingbeil (1998), the elastic release of constraints is equivalent to application of the biaxial bending moment $M = \int -\sigma_r(z)z\, dz$, which is related to the warping curvatures $w,_{xx} = w,_{yy} = \kappa$ through the elastic plate theory relation $\kappa = (1 - \nu)M/EI$. Note that the 1-D models can only predict equal and uniform curvatures in the x and y directions.

2-D Generalized Plane Strain (GPS) Models

The thermomechanical modeling procedures used for the GPS models are described in detail by Chin (1998), and are only briefly summarized here. The GPS model geometry and boundary conditions are depicted in Fig. 5. In short, each initially molten "row" of stainless steel (which corresponds to four deposited rows in the actual microcasting process) is successively bonded to the carbon steel substrate, with a 160 second delay between rows to approximate the real-time experiments. The generalized plane strain theory applied here assumes that the 2-D model lies between two rigid bounding planes which are orthogonal to the axial direction of the model (the x direction in Fig. 5). As opposed to plane strain, where the bounding planes are fixed, generalized plane strain allows relative rigid body movement between the two planes. Thus, the planes may undergo a relative uniform axial displacement u_x, as well as relative rotations per unit length ϕ_y and ϕ_z about the y and z axes, respectively. As for the 1-D models, the mechanical constraints of Fig. 5 are chosen to approximate the bolted constraints in the experiments (i.e., no warping). Thus, the right and left edges are constrained to be vertical, while the out-of-plane rotation ϕ_y is constrained to be zero. As for the 1-D models, three separate thermal boundary conditions on the bottom of the substrate are considered ($T = 30°C$, $T = 200°C$, and convection). Following deposition of the final row and cooling to room temperature, warping deformation is obtained in a separate solution step by releasing both the in-plane constraints and the out-of-plane constraint ϕ_y. As discussed by Klingbeil (1998), it is possible to obtain 3-D numerical plate deflections from the 2-D GPS in-plane deflections and out-of-plane rotation ϕ_y. Predicted $n = 2$ and $n = 3$ curvatures $w,_{xx}$ and $w,_{yy}$ are then obtained using the same 2-D polynomial least square fits applied to experimental displacement data.
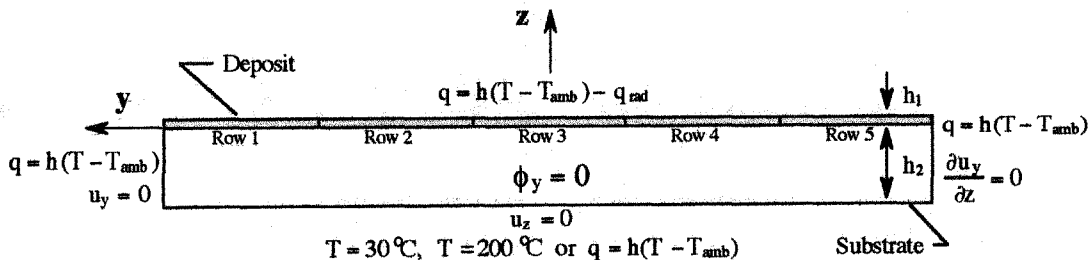

Figure 5. Generalized Plane Strain Geometry and Boundary Conditions

Representative Numerical Results

The 1-D axisymmetric and average ($n = 2$) GPS curvature results for each of the three thermal boundary conditions are given in Table 3. As seen in Table 3, the GPS curvatures in each

direction are for all cases substantially less than the 1-D model predictions. This result is consistent with the deposited row free-edge effects and inherent substrate heating accounted for in the generalized plane strain modeling, which suggests that the GPS models are closer to capturing the physical conditions present during actual material deposition. In addition, the trends in both sets of results with respect to the thermal boundary condition on the bottom are as expected. Namely, the T = 30°C condition results in the most warping, while the convection condition results in the least warping.

Table 3. Numerical Model Curvature Predictions

Thermal B.C. on Bottom	1-D Model κ / κ_{max}	GPS Average (n = 2) Curvatures	
		$w_{,xx} / \kappa_{max}$	$w_{,yy} / \kappa_{max}$
T = 30°C	0.819	0.661	0.689
T = 200°C	0.515	0.371	0.472
Convection	0.257	0.134	0.186

(Note: $\kappa_{max} = 0.00834$ in^{-1})

As previously mentioned, the thermomechanical models are designed to capture residual stresses in microcasting. A comparison of Tables 1 and 3 indicates that for both the 1-D and GPS models, the T = 30°C and convection conditions respectively serve as upper and lower bounds on the measured microcast results. In addition, both the 1-D and GPS numerical models indicate that the T = 200°C condition offers substantially less warping than the T = 30°C condition, which supports the observation that substrate preheating results in less warping. With respect to a difference in warping in the two directions, however, the GPS results do not agree with the measured observations. Furthermore, n = 3 GPS curvature results (not shown here) were unable to capture the variation in $w_{,yy}$ observed in the raster path experiments. As discussed by Klingbeil (1998), the discrepancies between trends in the GPS and measured results can be attributed to the out-of-plane constraints of the GPS models coupled with large-scale elastic-plastic deformation during manufacture. In brief, the GPS constraints result in severe interactions between rows, which when accompanied by large-scale nonlinear behavior can substantially affect the gradients in the out-of-plane stress distributions responsible for subsequent warping in the x direction. Such interactions could physically exist for rectangular plates which are long in the x direction, however such interactions are unlikely for square plates such as those used in the experiments.

Implications of the Numerical Results
The numerical results suggest that substrate pre-heating/insulating conditions can play an important role in direct metal deposition processes. Both the 1-D and GPS numerical models indicate that the T = 200°C condition offers substantially less warping compared to the T = 30°C condition, while the convection condition gives the least warping of all. Thus, the results suggest that a combination of uniform substrate pre-heating and thermal insulation beneath the substrate could be an effective means for reducing warping. Another important implication of the numerical results is evident from the discrepancies between the GPS models and the measured observations. Namely, the generalized plane strain models indicate that when modeling high-temperature nonlinear material response, the role of constraints is vitally important. This suggests that constraints used during actual material deposition (i.e., exactly how the part is secured during manufacture) may have a measurable effect on subsequent warping.

Conclusions
Residual stress-induced warping is perhaps the most fundamental obstacle to overcome in direct layered manufacturing of fully-dense metal parts. From this work two major conclusions can be made, which are relevant to SDM and other SFF processes. First, it appears that a

combination of substrate preheating (to reduce initial thermal mismatches) and substrate insulation (to exploit preheating by the process itself) could give substantial payoffs in limiting residual stress-induced warping. This is in contrast to active, controlled part heating throughout the deposition process, which would be cumbersome and costly to implement. Previous work by the authors has demonstrated the importance of constraining parts from warping during manufacture to limit warping deflections in finished parts. The results of this study further suggest that maintaining 3-D mechanical constraints that are consistent from part to part is also important. Because of large-scale thermoplastic deformation during manufacture, small changes in part constraints can result in unacceptable changes in warping deformations. Specifically, results in this study suggest that subtle changes in 3-D part constraints can reverse directional differences in warping seen as a result of deposition path.

Acknowledgments

References

Amon, C.H., Beuth, J.L., Merz, R., Prinz, F.B. and Weiss, L.E., 1998, "Shape Deposition Manufacturing with Microcasting: Processing, Thermal and Mechanical Issues," *Journal of Manufacturing Science and Engineering*, in print.

Chin, R.K., 1998, "Thermomechanical Modeling of Residual Stresses in Layered Manufacturing with Metals," Ph.D. Thesis Dissertation, Carnegie Mellon University.

Chin, R.K., Beuth, J.L. and Amon, C.H., 1996a, "Thermomechanical Modeling of Molten Metal Droplet Solidification Applied to Layered Manufacturing," *Mechanics of Materials*, Vol. 24, 257-271.

Chin, R.K., Beuth, J.L. and Amon, C.H., 1996b, "Thermomechanical Modeling of Successive Material Deposition in Layered Manufacturing," *Proc. 1996 Solid Freeform Fabrication Symposium* (D.L. Bourell, J.J. Beaman, H.L. Marcus, R.H. Crawford, and J.W. Barlow, eds.), Austin, August 1996, 507-515.

Chin, R.K., Beuth, J.L. and Amon, C.H., 1995, "Control of Residual Thermal Stresses in Shape Deposition Manufacturing," *Proc. 1995 Solid Freeform Fabrication Symposium* (H.L. Marcus, J.J. Beaman, D.L. Bourell, J.W. Barlow and R.H. Crawford, eds.), Austin, August 1995, 221-228.

Fessler, J.R., Merz, R., Nickel, A.H. and Prinz, F.B., 1996, "Laser Deposition of Metals for Shape Deposition Manufacturing," *Proc. 1996 Solid Freeform Fabrication Symposium* (D.L. Bourell, J.J. Beaman, H.L. Marcus, R.H. Crawford, and J.W. Barlow, eds.), Austin, August 1996, 117-124.

Klingbeil, N.W., 1998, "Residual Stress-Induced Warping and Interlayer Debonding in Layered Manufacturing," Ph.D. Thesis Dissertation, Carnegie Mellon University.

Klingbeil, N.W., Zinn, J.W. and Beuth, J.L., 1997, "Measurement of Residual Stresses in Parts Created by Shape Deposition Manufacturing," *Proc. 1997 Solid Freeform Fabrication Symposium* (D.L. Bourell, J.J. Beaman, R.H. Crawford, H.L. Marcus, J.W. Barlow, eds.), Austin, August 1997, 125-132.

Merz, R., Prinz, F.B., Ramaswami, K., Terk, M. and Weiss, L.E., 1994, "Shape Deposition Manufacturing," *Proc. 1994 Solid Freeform Fabrication Symposium* (H.L. Marcus, J.J. Beaman, J.W. Barlow, K.L. Bourell and R.H. Crawford eds.), Austin, August 1994, 1-8.

Prinz, F.B., *et al.*, 1997, *JTEC/WTEC Panel Report on Rapid Prototyping in Europe and Japan, Vol. 1,* Rapid Prototyping Association of the Society of Manufacturing Engineers, 1997.

Prinz, F.B, Weiss, L.E., Amon, C.H. and Beuth, J.L., 1995, "Processing, Thermal and Mechanical Issues in Shape Deposition Manufacturing," *Proc. 1995 Solid Freeform Fabrication Symposium* (H.L. Marcus, J.J. Beaman, D.L. Bourell, J.W. Barlow and R.H. Crawford, eds.), Austin, August 1995, 118-129.